Environmental Science & Technology

pubs.acs.org/est

Article

Olivine-Induced Alkalinity Enhancement Amplifies Phytoplankton Carbon Export Efficiency

Published as part of Environmental Science & Technology special issue "Ocean Health".

Xin Lin,* Canru Li, David A. Hutchins, Haodong Luo, Ningxin Yan, Yan Li, Yuan Jiang, Zhimian Cao, and Minhan Dai

Cite This: https://doi.org/10.1021/acs.est.6c02131

Read Online

ACCESS | Metrics & More | Article Recommendations | Supporting Information

ABSTRACT: Ocean alkalinity enhancement (OAE) via olivine addition is a promising carbon dioxide (CO_2) removal strategy, yet its impact on phytoplankton-driven biogeochemical processes remains unclear. We investigated the effects of olivine on the diatom *Thalassiosira pseudonana* (*T. pseudonana*) and the coccolithophore *Emiliania huxleyi* (*E. huxleyi*;calcifying and noncalcifying strains). Olivine addition increased total alkalinity across all cultures, although the increase was less pronounced in calcifying *E. huxleyi*. Notably, olivine stimulated growth and particulate organic carbon production in *T. pseudonana* and calcifying *E. huxleyi*, while noncalcifying strains showed no significant response. Olivine addition dramatically accelerated sinking rates, which increased 9.36-fold for *T. pseudonana* and 2.39-fold for calcifying *E. huxleyi*. This enhancement was driven by distinct mechanisms: silicon-mediated ballasting in diatoms and extracellular polysaccharide-induced cell−olivine aggregation in coccolithophores, alongside minor silicon deposition on coccoliths. These results indicate that olivine-based OAE could increase CO_2 drawdown through two independent mechanisms and may potentially strengthen the biological pump by accelerating organic matter export. Our findings suggest that olivine addition could serve as a potent approach for enhancing carbon export efficiency, with diatoms exhibiting a stronger response than coccolithophores, although its ecological impacts will require further investigation.

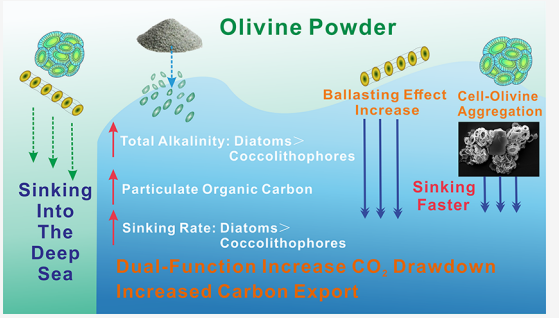

KEYWORDS: *carbon export, ocean alkalinity enhancement, olivine, phytoplankton, sinking rate*

1. INTRODUCTION

Ocean alkalinity enhancement (OAE) involves artificially enhanced weathering of alkaline materials, resulting in an increase in seawater total alkalinity (TA) and CO_2 uptake, thereby both sequestering carbon and counteracting ocean acidification.[1] Olivine is recognized as one of the most promising minerals for OAE due to its theoretical high CO_2 absorption efficiency and widespread availability.[2]

Marine phytoplankton play a crucial role in the global carbon cycle by carrying out half of all photosynthetic carbon fixation,[3] so it is essential to fully understand their likely responses to any contemplated OAE efforts. Coccolithophores and diatoms are ecologically and biogeochemically dominant primary producers. Coccolithophores are the major producers of biogenic calcite ($CaCO_3$) in the oceans,[4] while diatoms are pivotal in regulating the ocean's biogenic silica (BSi) cycle and are key exporters of particulate organic carbon (POC) within the marine ecosystem.[5]

Bach et al. speculated that the implementation of OAE using olivine might lead to a proliferation of diatoms and a decline in coccolithophore populations.[6] Recent laboratory studies have highlighted significant benefits to the diatom *Thalasiossira pseudonana* (*T. pseudonana*) from the silicate and iron released by olivine dissolution.[7,8] Another study also indicated that artificially synthesized olivine leachate had positive effects on the diatoms *Ditylum brightwellii* and *Nitzschia punctata*.[9] Li et al.[7] found that olivine particle addition enhanced the growth of the coccolithophore *Gephyrocapsa oceanica*, although the impact was not as pronounced as with diatoms. Similar results were observed with artificially synthesized olivine leachate and the coccolithophore *Emiliania huxleyi* (*E. huxleyi*;*Gephyrocapsa huxleyii*).[9] In contrast, an artificial alkalinization solution comprising Na_2CO_3 and $CaCl_2H_4O_2$ had neutral effects on the growth rates and elemental ratios of the coccolithophore *E. huxleyi* and the diatom *Chaetoceros* sp.[10]

A fraction of the biomass produced by phytoplankton photosynthesis sinks, exporting carbon to the deep ocean and

Received: February 9, 2026
Revised: March 10, 2026
Accepted: March 11, 2026

potentially to the ocean sediments for centuries to millennia.[11] This process is influenced by phytoplankton community structure, POC remineralization by bacteria and zooplankton,[12] and a suite of other environmental factors.[13,14] Rapid sinking is essential for the effectiveness of this oceanic "biological carbon pump." Slow sinking rates result in rapid, shallow bacterial decomposition of phytoplankton-derived POC, either converting carbon into dissolved organic matter or releasing it as CO_2.[15,16]

The "ballasting effect" is driven by relatively dense, mineral-rich particles from silicified diatoms and calcified coccolithophores accelerating the sinking rates of oceanic organic matter.[17] Even a 1% increase in the density of phytoplankton can double the sinking speed.[18] The frustules of diatoms are composed of $SiO_2 \cdot nH_2O$ and thus have low solubility and a higher density (2.1−2.3 g/cm^3) than seawater, which allows them to sink quickly and contributes significantly to the ocean carbon sink.[19−5] Coccolithophores generate calcite-coccoliths on their cell walls, which have a density even greater than silica relative to seawater (2.7 g/cm^3), facilitating rapid sinking of any associated POC. Coccolithophores are a primary driver of the "carbonate pump," which converts seawater bicarbonate into CO_2 through calcification, which lowers dissolved inorganic carbon (DIC) concentrations in the upper ocean while simultaneously leading to the evasion of CO_2 from the ocean to the atmosphere.[21] The opposing processes of primary production and calcification in coccolithophores can be represented by the ratio of particulate inorganic carbon (PIC) to POC. The PIC/POC ratio reflects the balance between calcification and photosynthesis and determines whether their growth acts as a net CO_2 sink or source.[22,23] The calcification process in coccolithophores leads to a decrease in seawater TA, which may counteract the effects of the OAE that aim to increase alkalinity. On the other hand, an increase in alkalinity due to OAE could potentially influence calcification, which in turn might affect the carbon sink through coccolithophores.[6] The interplay between OAE and calcification remains poorly understood and requires further exploration.

In this study, we assess biogeochemical and physiological responses to olivine addition in representative species of two ecologically significant phytoplankton groups: the coccolithophore *E. huxleyi* and the diatom *T. pseudonana*, with attention to changes in their sinking rates. Both calcifying and noncalcifying *E. huxleyi* strains were used to elucidate the interplay between alkalinity enhancement resulting from olivine addition and the process of calcification. Our findings are intended to shed new light on the biogeochemical effects of olivine addition on these key phytoplankton groups and their roles in the ocean carbon cycle.

2. MATERIALS AND METHODS

2.1. Composition and Particle Characteristics of Olivine Particles

The theoretical chemical equation of olivine dissolution is $(Mg, Fe)_2SiO_4 + 4H_2O + 4CO_2 = 2(Mg^{2+}/Fe^{2+}) + 4HCO_3^- + H_4SiO_4$.[24] The exact mineralogical composition depends on the olivine source, with the primary variations occurring in trace metal (e.g., Ni, Co, Cr) concentrations. We procured natural olivine particles (1−3 mm in diameter) from 3A Materials (CAS: 15118-03-3) and ground them using a QM-3SP2 planetary ball mill. The resulting olivine particles, with particle size quantiles of $D10$ = 1.520 μm, $D50$ = 6.135 μm, and $D90$ = 22.439 μm, featured a molar Fe-to-Mg ratio of 0.08:0.92, indicating a forsterite-92 (Fo92) composition. Further details on the olivine's composition and particle characteristics are provided in Tables S1 and S2.

2.2. Phytoplankton Cultivation and Experimental Design

The calcifying *E. huxleyi* (CCMP 1516, morphotype A), designated as *E. hux* (Cal), was isolated from the Equatorial Pacific (02.6667S, 82.7167W). The noncalcifying *E. huxleyi* strain CCMP 2090, designated as *E. hux* (noncal), was derived from CCMP 1516. In the ocean, noncalcifying coccolithophores are present but far less abundant than their calcifying counterparts.[25] Coccolith formation is influenced by environmental factors and can cease under specific conditions, as reported for *E. huxleyi* var. *aurorae*.[26] In laboratory cultures, nutrient-replete conditions (N or P) can induce the noncalcifying form of *E. huxleyi*.[27] Therefore, the noncalcifying strain used in this study likely resulted from similar nutrient-replete conditions. *T. pseudonana* (CCMP 1335, isolated from Moriches Bay [Long Island, New York]) was obtained from the Center for Collections of Marine Bacteria and Phytoplankton, designated as T. p. The phytoplankton were grown in triplicate polycarbonate containers filled with 2 L of Aquil artificial seawater[7] at an initial density of 2 × 10^4 cells per milliliter. Prior to the experiment, artificial seawater was first aerated with ambient air to ensure stability of the artificial seawater−carbonate system. The basal artificial seawater medium was identical for all of the strains. Silicic acid was added solely to *T. pseudonana* cultures to meet its obligate silicon requirement for growth, a condition not required by the coccolithophore strains. Therefore, any differential effects of olivine addition on parameters can be meaningfully compared between the species.[7] 0.2 g of olivine particles was introduced into the 2 L phytoplankton cultures. Phytoplankton cultures without olivine additions were used as the control. The containers for phytoplankton cultures were capped with air-permeable films (0.2 μm pore size, 85% air permeability, BKMAM) to ensure efficient gas exchange. The phytoplankton cultures were grown at 20 °C and illuminated with saturating cool-white fluorescent lighting at a photon flux intensity of 110 μmol photons m^{-2} s^{-1} with a 12:12 h light: dark cycle (n = 3). Aliquots were taken at 24, 72, 96, 144, and 192 h to measure biological and chemical parameters.

2.3. Measurement of Cell Concentration, Chlorophyll *a*, and Photochemical Efficiency

The cell abundance was measured by a flow cytometer (CytoFLEX S, Beckman Coulter, USA) after filtration through 30 μm innovative cell filters (CellTrics, Germany). To measure the Chlorphyll *a* concentration, samples were extracted using 5 mL of methanol at 4 °C overnight in the dark. After centrifugation at 8000 *g* for 10 min, the optical absorption of the supernatant was measured at 632, 665, and 750 nm by using a scanning spectrophotometer (DU 800, Beckman, USA). The Chl *a* concentration was then calculated using the equation of Ritchie (2006).[28]

2.4. Carbonate System Parameters and $SiOH_4$ Concentration Measurement

An AS-ALK2 TA titrator was used to measure the amount of TA in the samples (Apollo SciTech, USA) with a precision of better than ±2 μmol kg^{-1}. An AS-C3 total DIC analyzer was used to determine the amount of total DIC in the samples (Apollo SciTech, USA) with a precision of better than ±2 μmol kg^{-1}. Both DIC and TA measurements were calibrated with the certified reference material provided by Dr. Andrew Dickson of the Scripps Institution of Oceanography to achieve an accuracy better than ±2 μmol kg^{-1}. The concentrations of HCO_3^-, CO_2 (aq), pCO_2, $_\Omega$Ca, pH, and CO_3^{2-} were calculated by CO2SYS-v2.3 (a standalone program in the form of an Excel macro spreadsheet). An automatic nutrient analyzer (AA3, SEAL, Germany) was used to determine the $Si(OH)_4$ concentrations of samples with a precision of ±3% (1 standard deviation, 1 SD).

2.5. Particulate C, N, and BSi Measurement

The concentrations of POC and particulate organic nitrogen (PON) were measured using an Elementar Vario EL cube (Vario EL cube,

https://doi.org/10.1021/acs.est.6c02131
Environ. Sci. Technol. XXXX, XXX, XXX−XXX

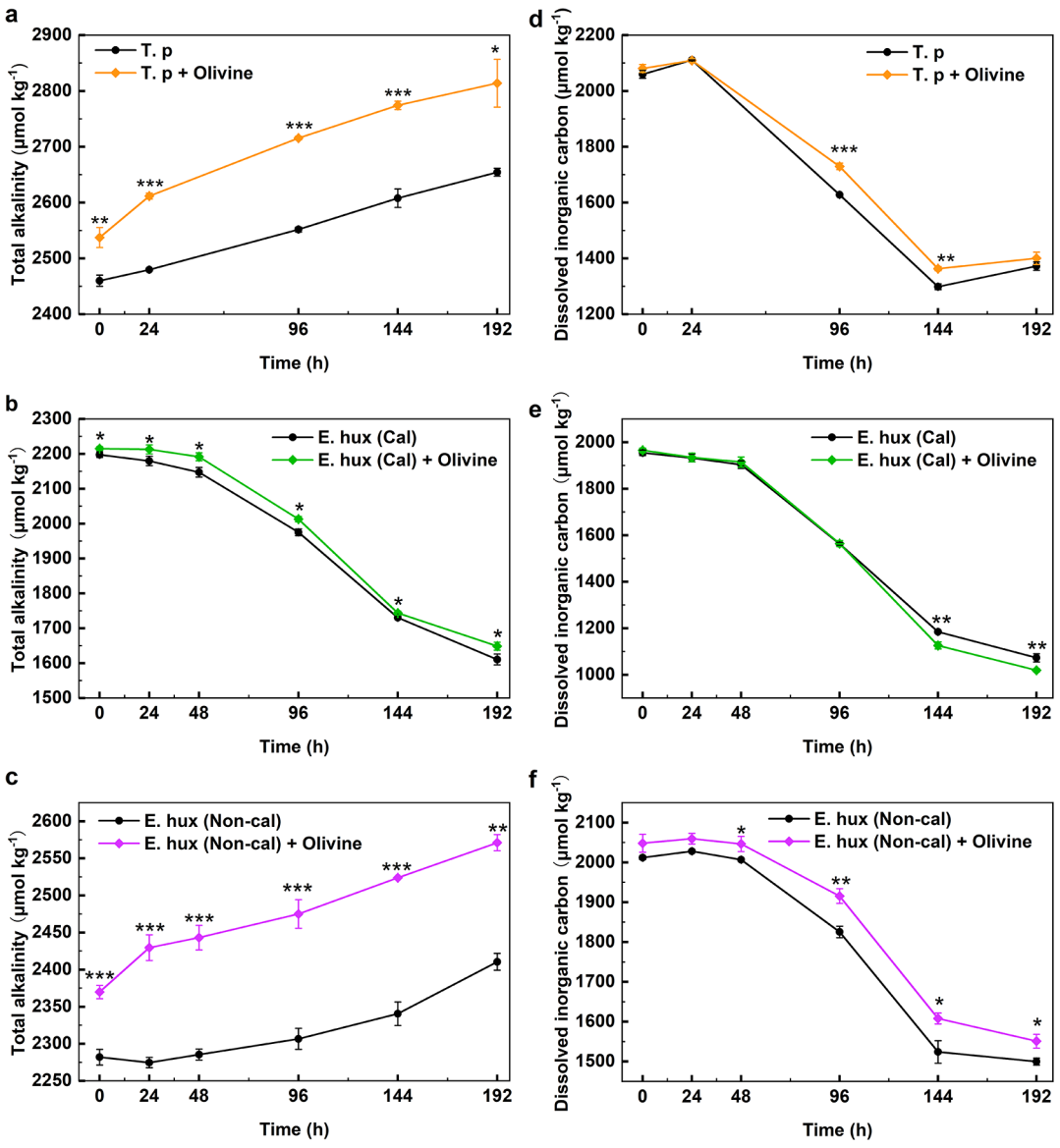

Figure 1. Changes in TA of *T. pseudonana* (T. p) (a), calcifying *E. huxleyi* (E. hux) (cal) (b), and noncalcifying *E. huxleyi E. hux* (cal) (c) during the culture of three phytoplankton strains with and without olivine addition during the cultivation. Changes in DIC concentrations of *T. pseudonana* (T. p) (d), calcifying *E. huxleyi, E. hux* (cal) (e), and noncalcifying *E. huxleyi E. hux* (Noncal) (f) with or without olivine during the cultivation. Data are presented as the mean ± SD (n = 3). Significant changes between treatments are shown as symbols (*p < 0.05; **p < 0.01; *** p < 0.001). Note that the measured TA at the nominal '0 h' already varied across treatments, as the initial rapid dissolution burst of olivine occurred during the sample collection window.

Elementar, Langenselbold, Germany) with a precision of < ±2% (1SD) for C and 5% (1SD) for N. The phytoplankton cultures were filtered through Whatman GF/F filters (25 mm) that had been precombusted at 450 °C for 5 h, then stored at −20 °C pending analysis. The filters used for POC analysis were treated with HCl to eliminate PIC. Conversely, the samples used for total particulate carbon (TPC) analysis were not treated with HCl. PIC was calculated as the difference between TPC and POC. The samples for BSi measurement were collected on polycarbonate membranes using a vacuum filtration pump (<0.01 MPa). The samples were then transferred into 15 mL centrifuge tubes and dried in an oven (DHG-9146A, Jing Hong, China) at 60 °C. For BSi extraction, 4 mL of 0.2 M NaOH was added to each tube, followed by vortexing and incubation in a boiling water bath for 30−40 min. After cooling in an ice bath, the digestion was neutralized with 1 mL of 1 N HCl. BSi was determined using UV spectrophotometry with a UV spectrophotometer (DU800, Beckman, Fullerton, California, USA). BSi was quantified via a Na_2SiF_6 standard curve.

2.6. Determination of Sinking Rate

The sinking rate of phytoplankton was measured using the settling column (SETCOL) method during the light period at 120 h of cultivation. This technique is widely used for measuring the sinking rates of phytoplankton cells.[13,29−31] Vertically mounted settling tubes were used for sinking rate determinations, with a capacity of approximately 385 mL and a height of 0.59 m. After the samples were shaken (15 s of vortexing plus 15 s of inversion) to ensure a homogeneous initial suspension, they were transferred to settling columns for the sinking rate measurements. The sinking rates of cells were determined by measuring the cell or Chl *a* concentration at various vertical positions within the settling tubes, collected from different outlets following a 2−3 h settling period. Chl *a* concentration was considered a biomass index for the determination of sinking rates. The sinking rate was calculated according to the following equation:

https://doi.org/10.1021/acs.est.6c02131
Environ. Sci. Technol. XXXX, XXX, XXX−XXX

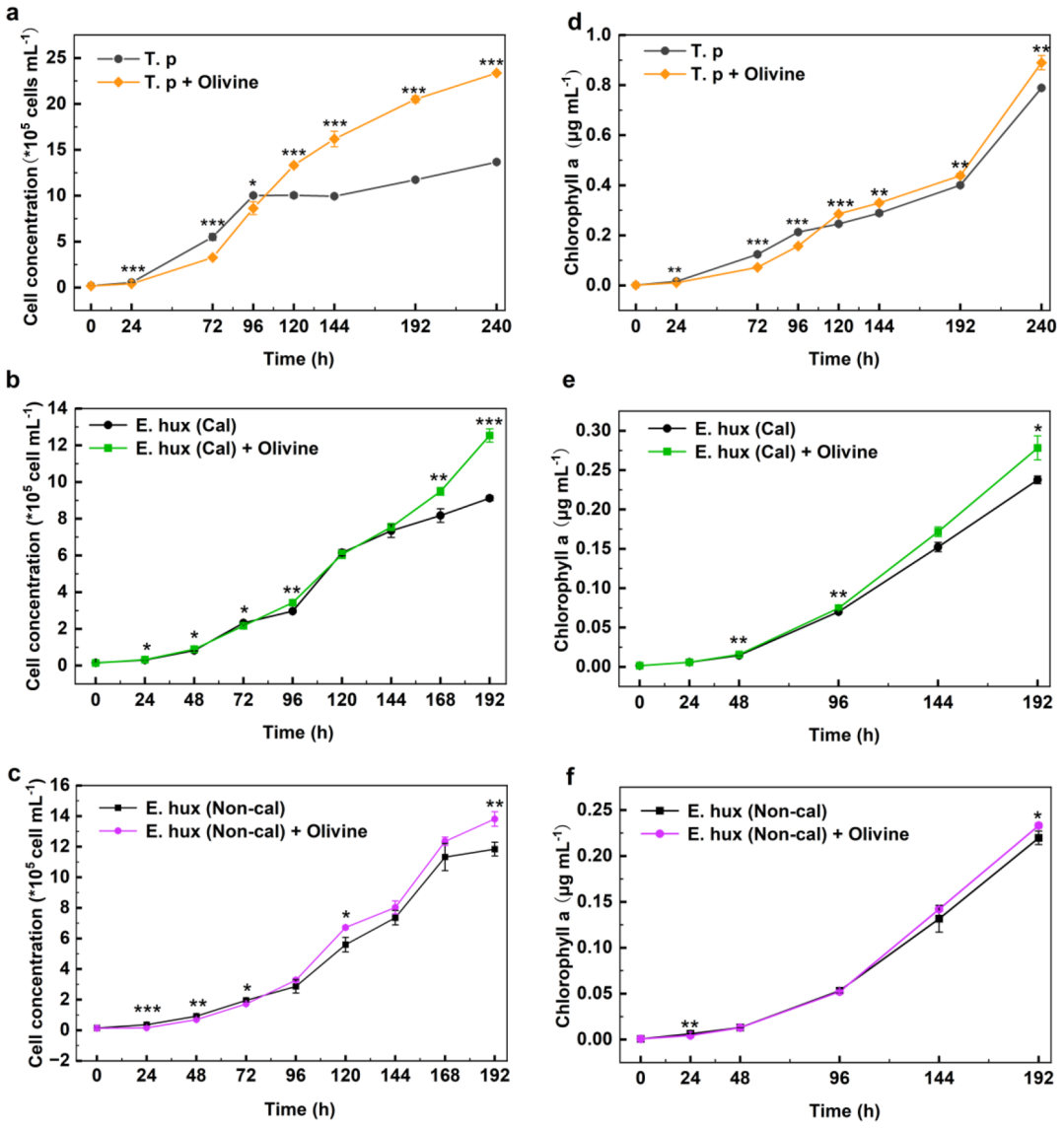

Figure 2. Changes in cell concentrations of *T. pseudonana* (T. p) (a), calcifying *E. huxleyi*, *E. hux* (cal) (b), and noncalcifying *E. huxleyi*, *E. hux* (noncal) (c) with or without olivine during cultivation. Changes in chlorophyll *a* concentration of *T. pseudonana* (T. p) (d), calcifying *E. huxleyi*, *E. hux* (cal) (e), and noncalcifying *E. huxleyi E. hux* (noncal) (f) with or without olivine during cultivation. Data are presented as the mean ± SD (n = 3). Significant changes between treatments are shown as symbols (*p < 0.05; **p < 0.01; *** p < 0.001).

$$V = \left(\frac{V_s \cdot b_s}{V_t \cdot \frac{b_{0,0} + b_{0,t}}{2}} - \frac{V_s}{V_t} \right) \cdot \frac{L}{t}$$

where V_s (mL) is the volume of the conical section, b_s is the Chl *a* concentration in the conical section at the end of the settling period, V_t (mL) is the total suspension volume, L (m) is the column height, and t is the sedimentation time. $b_{0,0}$ and $b_{0,t}$ represent the initial Chl *a* concentration and that after settling at the bottom, respectively.

2.7. Scanning Electron Microscopy Observation of Interactions of Olivine Particles with *E. huxleyi* and *T. pseudonana* and Compositional Analysis of *E. huxleyi* Coccoliths

Aliquots (10 μL) of calcifying *E. huxleyi* and *T. pseudonana* cultures supplemented with olivine particles were collected, deposited onto poly-L-lysine (PLL)-coated glass coverslips (1 cm × 1 cm), and incubated in a humidified chamber at room temperature for 1 h. PLL, a cationic amino acid polymer, is commonly used to coat glass slides for cell immobilization by electrostatic adhesion to negatively charged surfaces for microscopic observation without influencing biological processes or pre-existing cell−olivine interactions.[34] Subsequently, the samples were dehydrated through a graded ethanol series, with sequential 10 min immersions in 30, 50, 70, 90, and 100% (absolute) ethanol solutions. Following dehydration, the samples underwent critical point drying and were then sputter-coated with a gold−palladium (Au/Pd) alloy. Visualization of olivine particle interactions with *E. huxleyi* and *T. pseudonana* was performed using a Zeiss HD scanning electron microscope (SEM, FEI Quanta 650 FEG). Energy-dispersive X-ray spectroscopy (EDS) coupled with SEM was utilized to characterize the structural morphology and elemental composition of *E. huxleyi* coccoliths.

2.8. Statistical Methods

An analysis of variance (ANOVA) was employed to assess the statistical significance of the differences across various treatments. Significance was established at the p < 0.05 threshold. Subsequent to the ANOVA, Tukey's honestly significant difference test was applied for post hoc analysis to identify specific pairwise contrasts that were significantly different.

https://doi.org/10.1021/acs.est.6c02131
Environ. Sci. Technol. XXXX, XXX, XXX−XXX

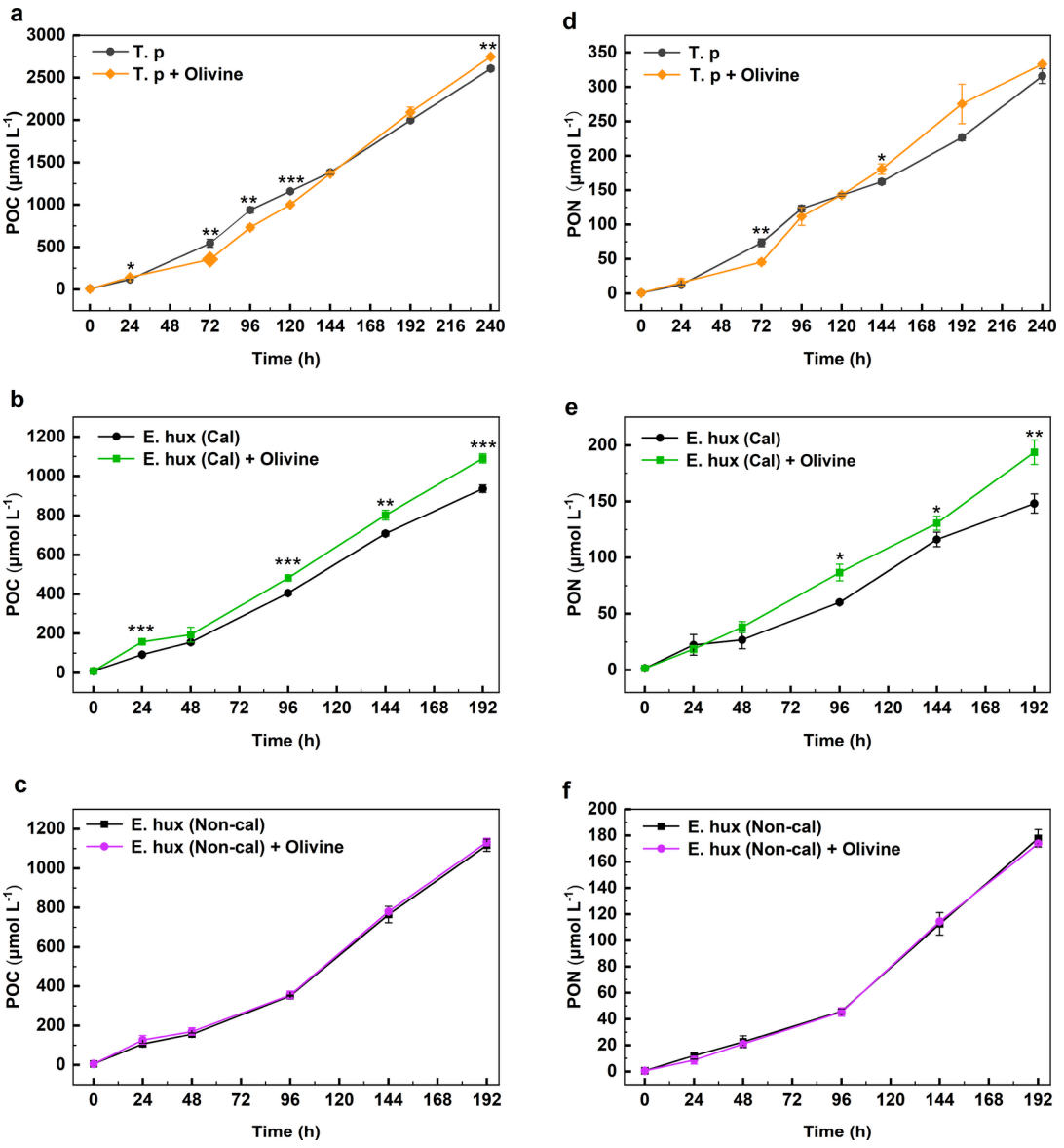

Figure 3. POC content per liter of *T. pseudonana* (T. p) (a) calcifying *E. huxleyi*, *E. hux* (Cal) (b), and noncalcifying *E. huxleyi E. hux* (Noncal) (c) cultures (per liter) with or without olivine during cultivation. Changes in PON content per liter of *T. pseudonana* (T. p) (d), calcifying *E. huxleyi*, *E. hux* (Cal) (e), and noncalcifying *E. huxleyi*, *E. hux* (Noncal) (f) cultures with or without olivine during the cultivation. Data are presented as the mean ± SD (n = 3). Significant changes between treatments are shown as symbols (*p < 0.05; **p < 0.01; *** p < 0.001).

3. RESULTS

3.1. Effects of Olivine Addition on the Carbonate System of Phytoplankton Cultures

TA increased in *T. pseudonana* and noncalcifying *E. huxleyi* cultures but decreased in calcifying *E. huxleyi* cultures during cultivation (Figure 1a–c). Offsets in T_0 alkalinity between the olivine-treated and control groups were observed, which can be attributed to the rapid olivine dissolution of the reactive amorphous surface layer of the artificially ground olivine particles upon contact with seawater[32,33] (Figure 1, Table S3). Olivine particles significantly enhanced TA in *T. pseudonana* and noncalcifying *E. huxleyi* cultures (Figure 1a,c). Specifically, in *T. pseudonana* cultures with olivine, TA was significantly elevated compared to controls without olivine (p < 0.05), with increases of 3.15, 5.32, 6.43, 6.38, and 6.01% (77.40–159.50 μmol kg^{-1}) at different time points. In the first 24 h, the TA in the olivine group increased by 74.17 μM, nearly four times the rate of the control (19.55 μM) (Figure 1a). Similarly, the noncalcifying *E. huxleyi* cultures with olivine addition showed a much larger increase in TA, reaching 6.8–7.83% (87.81–160.57 μmol kg^{-1}) higher levels at various time points compared to controls (p < 0.05) (Figure 1c). In calcifying *E. huxleyi*, however, the effect of the addition of olivine on TA enhancement was much weaker (Figure 1b). Although a subtle but consistent and significant increase in TA was observed relative to the control without olivine (p < 0.05), the increases were minor, ranging from 0.79 to 2.37% at different time points (Figure 1b).

Generally, the DIC levels decreased over the course of cultivation for all three phytoplankton cultures (Figure 1d–f). The *T. pseudonana* culture with olivine showed significantly higher DIC concentrations at 96 (5.80%) and 144 h (4.70%) (p < 0.05) compared to those without olivine (Figure 1d). In the calcifying *E. huxleyi* culture, olivine addition did not significantly increase DIC above control levels but instead

https://doi.org/10.1021/acs.est.6c02131
Environ. Sci. Technol. XXXX, XXX, XXX−XXX

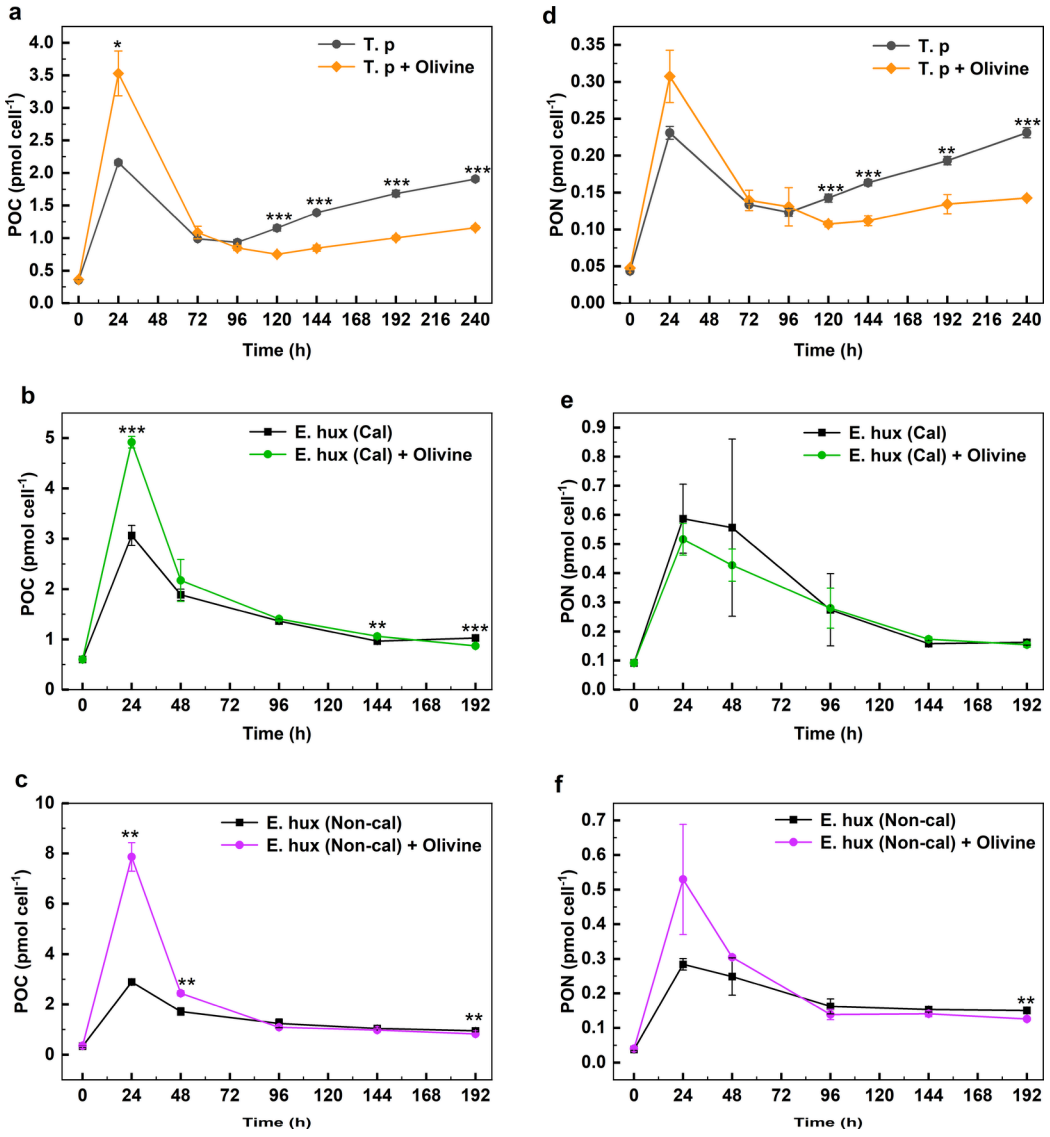

Figure 4. POC concentrations per cell of *T. pseudonana* (T. p) (a) calcifying *E. huxleyi*, *E. hux* (Cal) (b), and noncalcifying *E. huxleyi*, *E. hux* (Noncal) (c) with or without olivine during cultivation. Changes in PON concentrations per cell of *T. pseudonana* (T. p) (d), calcifying *E. huxleyi*, *E. hux* (Cal) (e), and noncalcifying *E. huxleyi*, *E. hux* (Noncal) (f) cultures with or without olivine during the cultivation. Data are presented as the mean ± SD (n = 3). Significant changes between treatments are shown as symbols (*p < 0.05; **p < 0.01; *** p < 0.001).

significantly decreased DIC at 144 and 192 h by 5.39 and 5.48%, respectively (p < 0.05) (Figure 1e). In the noncalcifying *E. huxleyi* culture, olivine addition maintained higher DIC levels relative to controls without olivine by 1.98, 4.94, 5.51, and 3.42% at 48, 96, 144, and 192 h (p < 0.05) (Figure 1f).

The addition of olivine resulted in a significant increase in the calcium carbonate saturation state ($_{\Omega}$Ca), pH, and the concentration of CO_3^{2-}, as well as a significant decrease in the concentration of dissolved CO_2 (aq) and partial pressure of CO_2 (pCO_2) in cultures of *T. pseudonana*, calcifying *E. huxleyi*, and noncalcifying *E. huxleyi* (p < 0.05) (Figures S1 and S2).

3.2. The Effects of Olivine Addition on Cell Abundance and Chl *a* Concentration

Adding olivine had more pronounced positive effects on the cell abundance of *T. pseudonana* compared to both calcifying and noncalcifying *E. huxleyi*. Cell concentrations in *T. pseudonana* cultures with olivine addition were slightly but significantly lower at early time points (24, 72, and 96 h) (Figure 2a). However, from 120 to 240 h, the group with olivine addition exhibited significantly higher concentrations, increasing by 32.70−74.81% (p < 0.05) (Figure 2a). The calcifying *E. huxleyi* with olivine addition showed significantly higher cell concentrations compared to the control group at various time points with increases of 6.75, 8.07, 15.45, 16.06, and 37.49%, respectively (p < 0.05, Figure 2b). Noncalcifying *E. huxleyi* exhibited higher cell concentrations without olivine addition between 24 and 72 h compared to the olivine-added group (p < 0.05). Conversely, from 96 to 192 h, the cell concentration of olivine-added noncalcifying *E. huxleyi* was higher than the control without olivine addition (p < 0.05) (Figure 2c). Olivine addition significantly increased the Chl *a* concentration in the late-stage *T. pseudonana* culture by 9.54−16.32% at different intervals (Figure 2d) and in the calcifying *E. huxleyi* culture by 6.96, 6.45, and 17.08% at 48, 96, and 192 h, respectively (Figure 2e). Significantly higher Chl *a* concentrations in noncalcifying *E. huxleyi* without olivine were observed at 24 h (p < 0.05), but no significant differences were detected at the late stage of cultivation (Figure 2f).

https://doi.org/10.1021/acs.est.6c02131
Environ. Sci. Technol. XXXX, XXX, XXX−XXX

3.3. The Effects of Olivine Addition on Organic Carbon and Nitrogen Content

The POC and PON concentrations per liter (μmol/L) in *T. pseudonana* and calcifying and noncalcifying *E. huxleyi* cultures exhibited distinct responses to olivine addition. In *T. pseudonana*, the POC concentration with olivine was 4.79% higher than that without olivine ($p < 0.05$), although the culture without olivine showed higher POC concentrations during the middle stage of cultivation (Figure 3a). In the calcifying *E. huxleyi*, the POC concentrations with olivine were significantly higher than those without olivine at 24, 96, 144, and 192 h ($p < 0.05$), with increases of 71.39, 19.02, 13.19, and 16.53%, respectively (Figure 3b). In contrast, no significant differences were observed in noncalcifying *E. huxleyi* (Figure 3c). The PON concentration in T. pseudonana with olivine was significantly higher at 144 h, with an 11.31% increase ($p < 0.05$), despite being higher without olivine at 72 h (Figure 3d). Similarly, the PON content with olivine was significantly higher at 96, 144, and 192 h, with increases of 44.10, 12.53, and 30.86%, respectively ($p < 0.05$) (Figure 3e). For noncalcifying *E. huxleyi*, no significant differences in PON concentrations were observed between cultures with and without olivine addition, except at 192 h, where the culture without olivine was slightly but significantly higher (Figure 3f). However, noncalcifying *E. huxleyi* generally had a higher POC content than calcifying *E. huxleyi* regardless of olivine addition (Figure 3b,f).

Significant increases in the POC concentration per cell (pmol/cell) were observed in *T. pseudonana*, calcifying *E. huxleyi*, and noncalcifying *E. huxleyi* after 24 h of olivine addition compared to the control without olivine (Figure 4 a–c). However, in *T. pseudonana*, significantly higher POC and PON concentrations per cell were observed in the control without olivine compared to the olivine-treated group during the late stage of cultivation (Figure 4a,d). In contrast, the differences in POC and PON concentrations per cell between the olivine-treated and control groups were minimal in both calcifying and noncalcifying *E. huxleyi* cultures (Figure 4b,c,e,f).

3.4. The Effects of Olivine Addition on $SiOH_4$ Concentration and BSi:POC of *T. pseudonana* and PIC:POC of *E. huxleyi*

The temporal dynamics of $Si(OH)_4$ concentration exhibited distinct patterns among different phytoplankton strains. The $Si(OH)_4$ concentrations were significantly higher in all cultures with olivine addition compared to the cultures without olivine addition (Figure 5). The $Si(OH)_4$ concentration in the *T. pseudonana* culture with olivine addition increased from 0 to 24 h but gradually decreased to a very low level. For the *T. pseudonana* culture without olivine addition, $Si(OH)_4$ concentration gradually decreased to a very low level, similar to the *T. pseudonana* culture with olivine addition (Figure 5a). In contrast, the $Si(OH)_4$ concentrations in calcifying and noncalcifying *E. huxleyi* cultures with olivine addition increased sharply from 0 to 48 h and remained elevated afterward. Notably, the noncalcifying strain exhibited 2.2-fold higher $Si(OH)_4$ concentrations than the calcifying strain at 192 h (86.79 vs 38.60 μmol/L; Figure 5b,c).

The BSi concentration per liter in the culture medium and per cell of *T. pseudonana* with olivine addition was significantly higher than that without olivine addition at most time points (Figure 6a,b). At 24 h, the olivine-treated samples exhibited

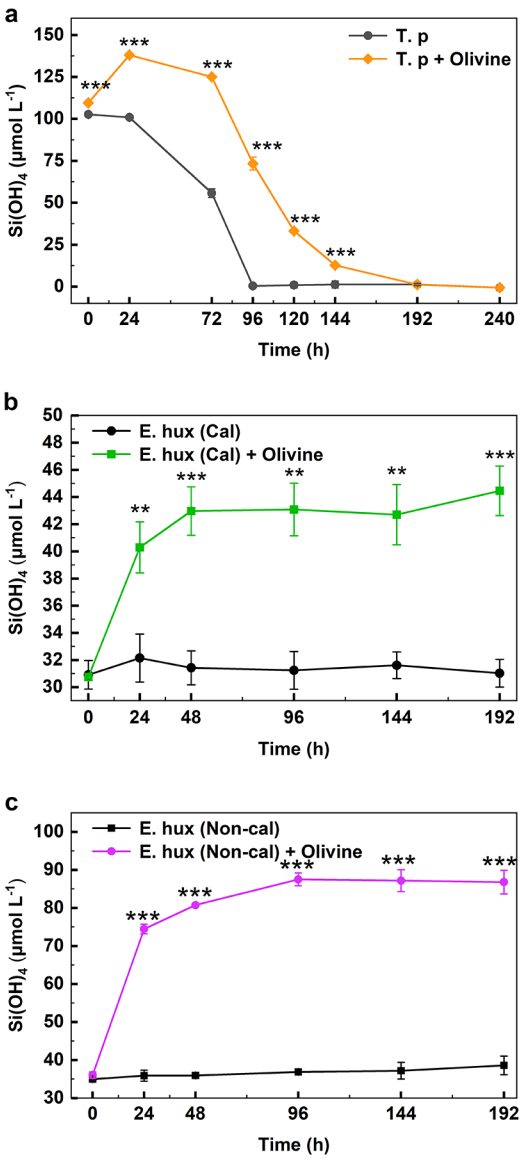

Figure 5. $Si(OH)_4$ concentration in the *T. pseudonana* (T. p) culture with and without olivine addition (a). Changes in $Si(OH)_4$ concentration in calcifying (b) and noncalcifying *E. huxleyi* (c) with and without olivine addition. Data are presented as the mean ± SD ($n = 3$). Significant changes between treatments are shown as symbols (*$p < 0.05$; **$p < 0.01$; *** $p < 0.001$).

unexpectedly high concentrations of measured BSi compared with the control. However, this was followed by a relative plateau between 24 and 72 h, despite the observed drawdown of $Si(OH)_4$ in the medium (Figure 6). Additionally, the BSi/POC ratio was also significantly higher with olivine addition from 24 to 240 h (Figure 6c), and the BSi was negatively correlated with POC in *T. pseudonana* (Figure S3).

At 96 h, the PIC content (μmol/L) of *E. huxleyi* without olivine addition was 2.04 times higher than that with olivine ($p < 0.01$). However, by 196 h, olivine-added cultures showed 24.24% higher PIC content (μmol/L) than controls ($p < 0.05$, Figure 6d). The cellular PIC was 2.38 times higher without olivine addition than in the olivine-added group at 96 h ($p < 0.01$, Figure 6e). At 96 h, the PIC/POC ratio was significantly higher without olivine addition than in the olivine-treated group, remaining consistently below 1 throughout the

https://doi.org/10.1021/acs.est.6c02131
Environ. Sci. Technol. XXXX, XXX, XXX−XXX

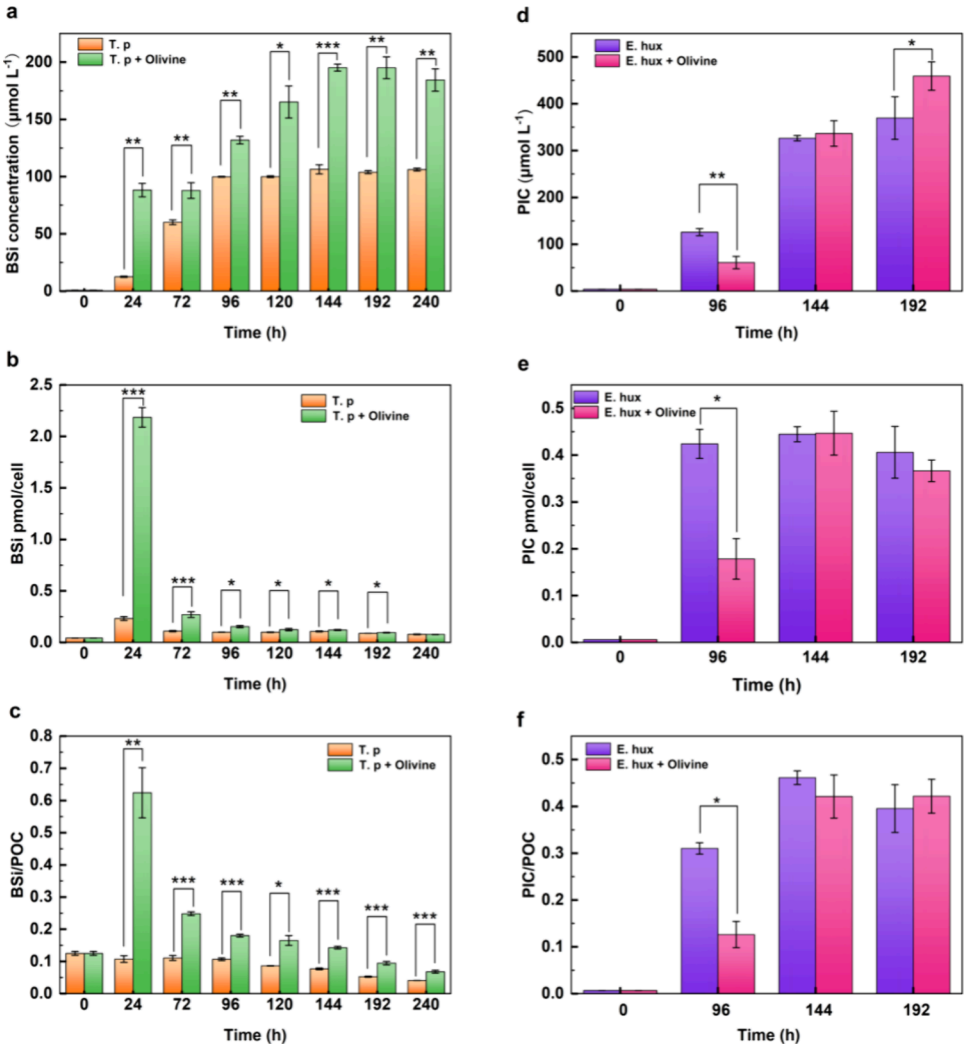

Figure 6. Changes of BSi in *T. pseudonana* and PIC in calcifying *E. huxleyi* with and without olivine addition. BSi concentration in *T. pseudonana* culture medium with and without olivine addition (a). BSi concentration per cell of *T. pseudonana* with and without olivine addition (b). BSi/POC ratio of *T. pseudonana* with and without olivine addition (c). PIC concentration of calcifying *E. huxleyi* with and without olivine addition during cultivation. PIC concentration of calcifying *E. huxleyi* culture medium with and without olivine (d). PIC concentration per cell of calcifying *E. huxleyi* with and without olivine (e). PIC/POC ratio of calcifying *E. huxleyi* with and without olivine (f). Data are presented as the mean ± SD (n = 3). Significant changes between treatments are shown as symbols (*p < 0.05; **p < 0.01; *** p < 0.001).

experiment (Figure 6f). A positive correlation between POC and PIC contents was observed in calcifying *E. huxleyi* (Figure S3).

3.5. The Effects of Olivine Addition on the Sinking Rate of *T. pseudonana* and Calcifying *E. huxleyi*

With olivine addition, the sinking rate (m d^{-1}) of *T. pseudonana* was significantly higher, being 9.64 times (Figure 7a) greater than without olivine (p < 0.05). Calcifying *E. huxleyi* with olivine addition also had a significantly higher sinking rate, with a 2.39-fold increase in those that used chlorophyll a concentration (p < 0.05) (Figure 7b). In contrast, the addition of olivine did not result in any significant changes to the sinking rate of noncalcifying *E. huxleyi* (Figure S4).

3.6. SEM Observations of Olivine Interaction with *E. huxleyi* and *T. pseudonana* and SEM-EDS Analysis on *E. huxleyi* Coccoliths

SEM observations demonstrated direct attachment of olivine particles to *E. huxleyi* cell surfaces, with EPS-like material bridging olivine particles and algal cells in the olivine-supplemented *E. huxleyi* cultures (Figure 7c,d). *T. pseudonana* showed no tendency to aggregate with olivine particles although EPS-like substances were observed on olivine surfaces in the *T. pseudonana* culture with olivine addition (Figure 7e,f).

Low silicon content was detected in distinct structural domains of *E. huxleyi* coccoliths via SEM-EDS (Figure 8). The Mg/Si ratio (weight-based) ranged from 0.91 to 1.88 among analyzed microregions, while the atomic Mg/Si ratio varied between 1.03 and 2.18. Similarly, the weight-based Mg/Ca ratio spanned 9.14−18.17, and the atomic Mg/Ca ratio ranged from 6.34 to 12.89. Although SEM-EDS provides semi-quantitative elemental analysis, the consistent detection of silicon across multiple measurement locations suggests some incorporation of Si into the coccolith structure.

4. DISCUSSION

This study demonstrates that olivine addition significantly enhances the sinking rates of *T. pseudonana* and calcifying *E. huxleyi*, suggesting its potential to improve the carbon transfer

https://doi.org/10.1021/acs.est.6c02131
Environ. Sci. Technol. XXXX, XXX, XXX−XXX

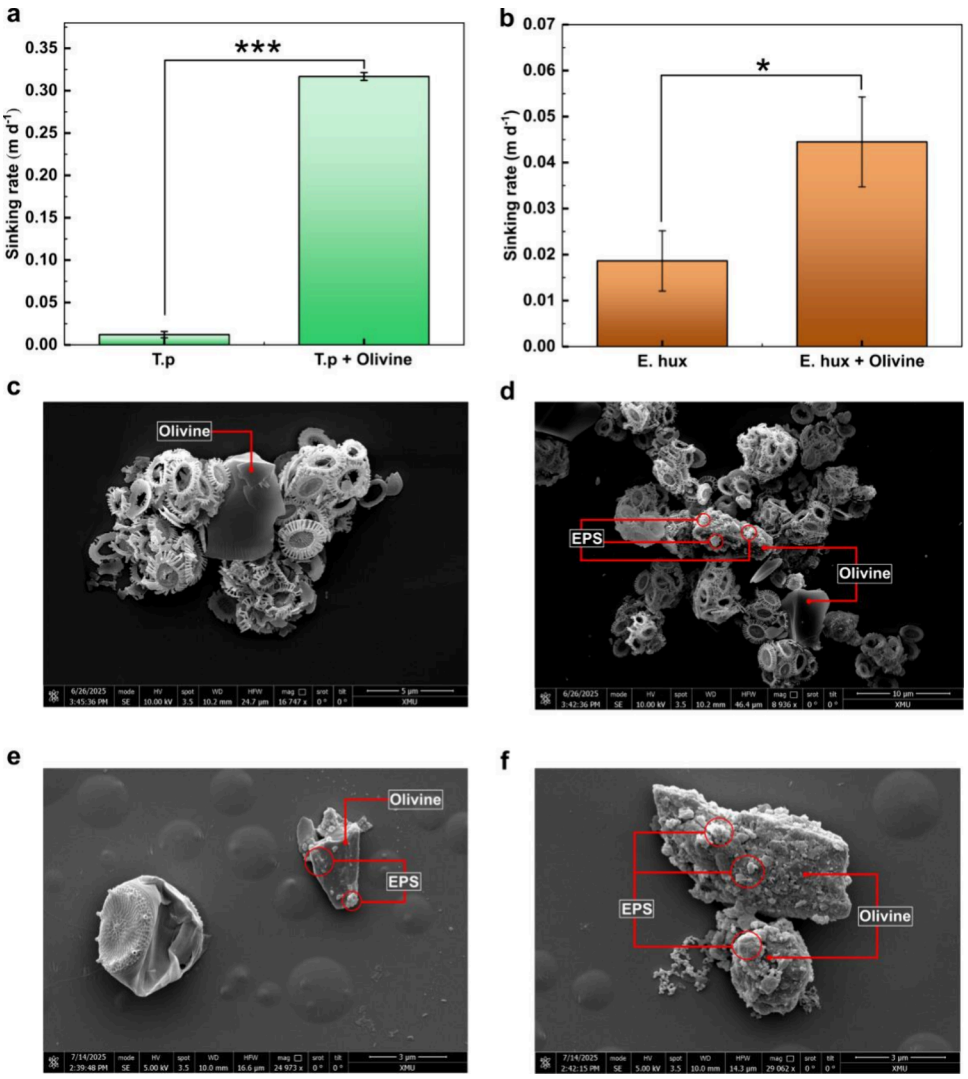

Figure 7. Sinking rates of *T. pseudonana* (T. p) (a) and calcifying *E. huxleyi* (E. hux) (b) with and without olivine addition based on the Chl *a* concentration. Data are presented as the mean ± SD ($n = 3$). Significant changes between treatments are shown as symbols (*$p < 0.05$; **$p < 0.01$; *** $p < 0.001$). SEM images revealed olivine particles attached to calcifying *E. huxleyi* cells (c, d), with extracellular polymeric substance (EPS)-like extracellular material present on the olivine particle surfaces in calcifying *E. huxleyi* culture with olivine addition (d). SEM images showing (EPS)-like extracellular material attached to the surface of olivine particles in the *T. pseudonana* culture with olivine addition (e, f).

efficiency to the deep ocean. Our findings further indicate that olivine may increase carbon removal efficiency in both diatoms and coccolithophores, with a more pronounced effect on diatoms.

Our study reveals that olivine addition significantly increased the cell concentration and Chl *a* concentration of the diatom and coccolithophores, with the most pronounced effects observed for the diatom *T. pseudonana* and the least pronounced effects on the noncalcifying *E. huxleyi*. These findings align with previous studies suggesting that silicon and iron released from olivine dissolution play key roles in promoting phytoplankton growth, with silicon particularly benefiting diatoms.[7,8] In addition to the direct chemical effects of olivine addition, the resulting higher phytoplankton cell density further decreased the concentration of dissolved CO_2. The lower initial Chl *a* and cell density in the olivine treatment were likely due to the light-shading effect of olivine particles. Olivine consistently promoted cell division rates after 120 h. At high growth rates, cells may prioritize division processes rather than pigment synthesis, which could account for the observed divergence between Chl *a* and cell concentrations after 120 h.

Olivine significantly enhanced POC and PON in calcifying *E. huxleyi* normalized by culture volume (μmol/L) but had negligible effects on noncalcifying *E. huxleyi* at later stages (Figure 3). We speculate that the increase in POC in calcifying *E. huxleyi* with olivine addition can be attributed to its indirect beneficial effects caused by enhanced calcification with olivine addition at a late stage of cultivation. Increased bicarbonate (HCO_3^-) from olivine dissolution, the primary carbon source for coccolithophore calcification,[35] likely enhanced calcification in calcifying *E. huxleyi* (Figure 6d). Calcification is energetically costly, consuming approximately one-third of the energy budget for photosynthesis,[36] which aligns with our findings that noncalcifying *E. huxleyi* exhibited higher POC content than its calcifying counterpart (Figure 3).[37] On the other hand, calcification has been shown to promote organic carbon sequestration by enhancing carbonate transport and increasing internal CO_2 availability for organic carbon fixation in *E. huxleyi*.[38] A positive correlation between POC and PIC

https://doi.org/10.1021/acs.est.6c02131
Environ. Sci. Technol. XXXX, XXX, XXX−XXX

a

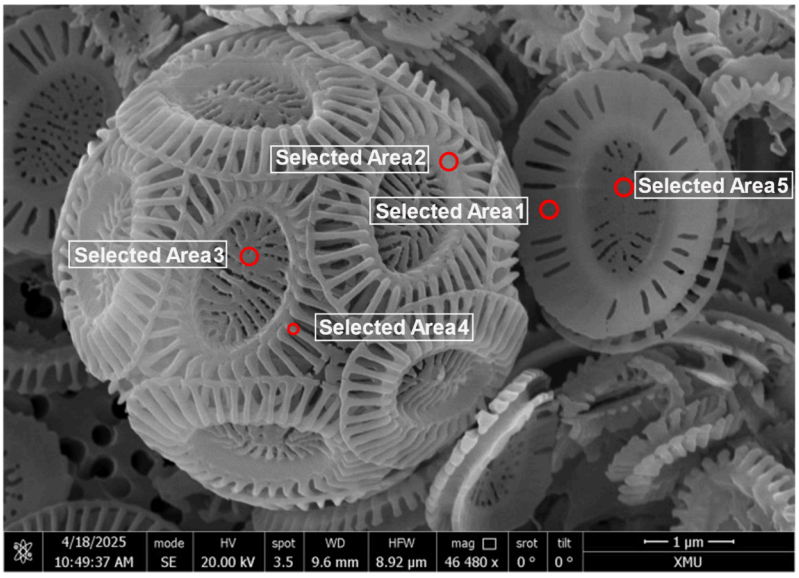

b

Selected Area	Weight% of Mg/Si	Atomic% of Mg/Si	Weight% of Ca/Si	Atomic% of Ca/Si	Error% of Mg	Error% of Si	Error% of Ca
1	1.09	1.26	12.56	8.78	26.22	27.33	6.83
2	1.88	2.19	18.17	12.89	15.21	15.23	4.24
3	1.18	1.34	9.14	6.34	17.80	13.21	6.05
4	1.00	1.14	11.92	8.30	22.59	21.59	5.45
5	0.91	1.04	9.74	6.75	32.44	30.70	8.44

Figure 8. Mg/Si and Ca/Si ratios of *E. huxleyi* coccoliths obtained from SEM-EDS analysis. SEM image showing five areas of *E. huxleyi* coccolith selected for EDS analysis (a). Mg/Si and Ca/Si ratios of the five areas. The reported "Error%" values represent the standard deviation of the quantitative EDS measurements, derived primarily from X-ray counting statistics (b).

contents observed in calcifying *E. huxleyi* in our study further supports the role of calcification in facilitating organic carbon fixation (Figure S2).

Olivine addition enhanced sinking rates by 9.64-fold in *T. pseudonana* and 2.39-fold in calcifying *E. huxleyi*, demonstrating significantly stronger effects on the diatom (Figure 7). The sinking rate of phytoplankton depends strongly on their "excess density"—the small but critical difference between cell/colony density and seawater density.[39] For example, seawater with a density of 1025 kg/m^3 (18 °C, 35 PSU) and phytoplankton with a density of 1035 kg/m^3 yield an excess density of 10 kg/m^3. It has been reported that an 8% density increase in the diatom *Conticribra weissflogii* (*Thalassiosira fluviatilis*) enhanced its sinking rate by 9.4-fold.[40] Based on SEM observations, which showed no production or aggregation of transparent exopolymeric particles (TEP) in our nutrient-replete diatom cultures, it is unlikely that the increased sinking rate was driven by higher cell abundance, leading to greater cell aggregation. Instead, the enhanced sinking rate was primarily attributed to the significant accumulation of biological BSi. Specifically, the olivine treatments maintained a markedly higher BSi concentration in comparison to the control. At 24 h, although amorphous olivine layers featuring highly reactive sites from initial grinding caused a transient abiotic BSi inflation (due to the kinetic similarity between amorphous minerals and BSi during NaOH extraction) in the olivine-added samples, this interference stabilized after 48 h, becoming negligible relative to the rapidly increasing biological signal. By 120 h, the measured BSi predominantly reflected authentic biological accumulation, overwhelming any residual abiotic background (Figure 6). This enhancement was driven by the synergistic coupling between diatom growth and olivine dissolution: while the high $Si(OH)_4$ concentrations in both treatments triggered nonsaturable, diffusion-driven uptake,[41] the biological removal of $Si(OH)_4$ by *T. pseudonana* cells accelerated olivine dissolution (as established in our previous work), fueling a positive feedback loop that further stimulated BSi accumulation. We therefore attribute the significantly enhanced sinking rate in *T. pseudonana* with olivine addition primarily to the elevated BSi content, which increased the cell density and thereby the ballast effect, a conclusion strongly supported by the increased BSi/POC ratios (Figure 6).

Olivine addition increased the sinking rate of calcifying *E. huxleyi*, though this was less pronounced than that for *T. pseudonana*. The PIC content did not increase with olivine addition (Figure 6), suggesting that alternative mechanisms contributed to the increased sinking rate. The silicon from olivine dissolution and its adhesion to or incorporation into the coccoliths of calcifying *E. huxleyi* likely partially accounts for the increased sinking rate. A lower concentration of $Si(OH)_4$ was observed in calcifying *E. huxleyi* cultures (44.46 µmol/L) compared to noncalcifying cultures (86.79 µmol/L) after 192 h of olivine addition (Figure 5). The $Si(OH)_4$ concentration in phytoplankton cell-free, olivine-added artificial seawater (86.13 µmol/L) matched that observed in noncalcifying *E. huxleyi* cultures.[7] This implies Si incorporation by calcifying *E. huxleyi*, though at rates far below those of the diatom *T. pseudonana* (Figure 5). Further evidence was from the EDS analysis, which demonstrated a low but detectable Si

https://doi.org/10.1021/acs.est.6c02131
Environ. Sci. Technol. XXXX, XXX, XXX−XXX

content in the coccoliths of calcifying *E. huxleyi* (Figure 8). This is aligned with previous observations using mass spectrometry.[42] The presence of silicon in the calcite exoskeletons of *E. huxleyi* was also confirmed by Ratcliffe et al.,[43] who suggested that it may play a role in facilitating calcification rather than serving as a structural component of the coccoliths. In a word, the low but detectable silicon incorporation by the calcifying *E. huxleyi* and the EDS-confirmed silicon deposition on coccoliths support the idea that olivine addition led to a slight increase in the cell mass of calcifying *E. huxleyi*.

Even minor Si incorporation into calcifying *E. huxleyi* could contribute to the increase of sinking rate since a 1% increase in the density of phytoplankton can double the sinking speed.[16] Based on the observed 48% lower $Si(OH)_4$ concentration in calcifying versus noncalcifying *E. huxleyi* cultures after 96 h (43.08 vs 87.50 μmol/L), this assimilation by calcifying *E. huxleyi* could increase cellular weight by approximately 1 pg/cell, resulting in an estimated excess density of 30 kg/m^3 ($\Delta\rho$ = m/V, assuming a spherical morphology with a mean cell diameter of 5 μm). Such density enhancement would account for the observed 2.4-fold increase in sinking rate (assuming a seawater density of 1025 kg/m^{-3} (18 °C, 35 PSU salinity) and a phytoplankton density of 1035 kg/m^{-3}). Given that coccolithophore densities typically surpass the generalized phytoplankton reference value (1035 kg/m^3), the density-driven component of sinking rate enhancement is likely less pronounced than the 2.4-fold projection.

Notably, coccolith-associated polysaccharides (CAPs), a specialized subclass of EPS in calcifying *E. huxleyi* with known adhesive properties,[44] likely mediated aggregation between calcifying *E. huxleyi* cells and olivine particles, likely contributing to the increased sinking rate of calcifying *E. huxleyi* with olivine addition. We observed direct adhesion of *E. huxleyi* cells to olivine particles with EPS-like coatings on mineral surfaces, further facilitating aggregation (Figure 7c,d). The significantly higher density of olivine particles compared to phytoplankton cells increases the overall density of the cell−olivine aggregates, thereby facilitating their sinking through a mechanism similar to clay flocculation in harmful algal bloom mitigation.[45] While representing a limitation for olivine-based alkalinity enhancement, incomplete olivine dissolution due to SiO_2 passivation[7] provides persistent ballast that could potentially enhance vertical flux, facilitating carbon export. The absence of aggregation between olivine particles and *T. pseudonana* cells, despite the presence of EPS on olivine surfaces (Figure 7e,f), highlights the potentially essential role of CAPs in mediating cell-mineral adhesion and aggregate formation.

Overall, olivine addition markedly enhanced the sinking rate of *T. pseudonana* via BSi enhancement, whereas the modest sinking rate increase in calcifying *E. huxleyi* can be explained by a slight incorporation of silicon into coccoliths (potentially increasing cell density), cell−olivine aggregation, and higher cell abundance that facilitated aggregation. These combined mechanisms collectively explain the enhanced sinking of calcifying *E. huxleyi* with olivine, while no such effect occurred in the noncalcifying strain due to the absence of coccoliths and associated CAPs (Figure S4). In the field, when coccolithophore concentrations are high, the likelihood of olivine particles attaching to the cells increases. Therefore, an olivine-driven OAE is expected to enhance the sinking rate of coccolithophores, particularly during blooms of this group.

In natural environments, diatoms readily form TEP, particularly under nutrient stress.[46] In contrast, coccolithophores do not typically form algal aggregates in natural environments, though they are often found in fecal aggregates.[47] Under our laboratory nutrient-replete conditions, TEP production by diatoms was not induced, which explains the lack of significant TEP observed in the diatom cultures. In a real-world application, adding olivine may enhance the sinking rate of diatoms by facilitating interactions between olivine particles and the TEP that diatoms naturally secrete.

The efficacy of the biological carbon pump depends on factors such as POC production, its decomposition by zooplankton and microorganisms, and the efficiency of POC transport to the deep sea.[11] Faster sinking of organic matter increases its likelihood of reaching the deep sea before decomposition and remineralization.[48] Furthermore, olivine-induced increases in BSi and POC could potentially enhance the export of POC not only from individual diatom and coccolithophore cells but also at the regional scale through incorporation into sinking aggregates and marine snow.[49,50]

The application of olivine in productive benthic ecosystems (100−300 g C m^{-2} yr^{-1})[51] and shallow waters may also shift the microalgal community toward a diatom-dominated assemblage, thereby potentially greatly increasing sinking carbon fluxes.[5] The fraction of water-column phytoplankton carbon production normally stored in shallow coastal and estuarine sediments has been estimated at ∼20%,[52] and our results suggest that it could be substantially higher with olivine additions. Although this enhanced sinking carbon flux due to olivine additions in nearshore waters is unlikely to reach the deep ocean, it may instead enhance organic carbon storage in shelf sediments as "Blue Carbon", albeit for a shorter duration than in the deep ocean.[53]

It is also important to consider whether excessively rapid sinking of phytoplankton could bring unintended ecological consequences. Greatly increased cellular sinking rates might have the potential to destabilize marine food webs through the precipitous declines of primary producers in surface waters. Further research will be needed both to determine the possible positive consequences of olivine additions for carbon sequestration and to test for any potential negative effects on nearshore food webs and biogeochemistry.

We propose that olivine addition may enhance carbon sequestration by diatoms through three mechanisms: (1) the increase in alkalinity from olivine addition, both directly through dissolution and indirectly via growth promotion ("enhanced alkalinity feedback effect"); (2) accelerating sinking rates ("more ballast feedback effect" mainly due to increased BSi); and (3) boosting organic carbon production ("more organic carbon feedback effect"). The elevated TA in the diatom-olivine system was synergistic. Olivine dissolution initially raised TA directly and indirectly promoted diatom growth. The resulting increase in biomass further enhanced TA and sustained olivine dissolution by inhibiting the formation of a passivating amorphous SiO_2 layer on olivine surfaces, thereby establishing a positive feedback loop.[7]

The effects of the addition of olivine on calcifying coccolithophores are more complex. Olivine addition enhances their sinking rates and POC production; however, the calcification process buffers against alkalinity increases, as evidenced by only a subtle increase in TA caused by olivine addition compared to *T. pseudonana* and noncalcifying *E. huxleyi* (Figure 1). Forming one mole of $CaCO_3$ reduces

https://doi.org/10.1021/acs.est.6c02131
Environ. Sci. Technol. XXXX, XXX, XXX−XXX

alkalinity by two moles, releasing CO_2, which offsets the alkalinity increase from olivine addition.[5] Although olivine addition increased the sinking rate and POC production in calcifying *E. huxleyi*, the negative impacts of increased calcification on alkalinity and CO_2 release need consideration. The actual ratio of CO_2 gas produced to precipitated $CaCO_3$ was reported to be 0.6 at 25 °C at the sea surface.[54] However, variability in CO_2/ PIC ratios under different conditions[55] introduces uncertainty in estimating CO_2 emissions from calcification. Thus, the net carbon sequestration effect depends on the balance between positive feedbacks (ballast and organic carbon effects) and negative impacts (reduced alkalinity and CO_2 release).[22]

In the future, we could consider integrating the "organic carbon feedback," "ballast feedback," and "less alkalinity feedback" processes into larger-scale models to better understand and predict the effects of olivine addition on the ecosystem. This integration is essential, as it enables the comprehensive consideration of the intricate biogeochemical processes that are initiated upon the application of an OAE in the ocean. Notably, olivine's rapid sinking and slow dissolution in deeper waters[56] limit its alkalinity release, prompting most OAE efforts to focus on shallow regions. Future improvements to olivine's sinking behavior could enhance its efficiency by prolonging surface dissolution.

Our findings and previous studies suggest that diatoms could potentially thrive with the addition of olivine for OAE, supporting the existing hypothesis.[6] The observed neutral effects of olivine addition on noncalcifying and nonsilicified phytoplankton were observed in our study using a noncalcifying strain of the coccolithophore *E. huxleyi* and olivine particles and with cyanobacteria species like *Synechococcus* sp., *Trichodesmium erythraeum*, and *Crocosphaera watsonii* using synthetic olivine leachate.[8] It appears that calcifying phytoplankton might experience greater benefits from olivine addition than noncalcifying species. It should be noted that the effects of olivine additions on phytoplankton may be diverse, as two decades of ocean acidification research have shown that perturbations in carbonate chemistry disproportionately affect phytoplankton.[57] In the future, enhancing our understanding of the ecological impacts of the OAE on phytoplankton communities will be vital for assessing the feasibility and potential for scaling up this proposed method for carbon dioxide removal from the atmosphere.

■ ASSOCIATED CONTENT

Supporting Information

The Supporting Information is available free of charge at https://pubs.acs.org/doi/10.1021/acs.est.6c02131.

Additional supplementary tables (Tables S1−S3) and figures (Figures S1−S4) regarding olivine characterization, seawater−carbonate chemistry, and phytoplankton physiological parameters (PDF)

■ AUTHOR INFORMATION

Corresponding Author

Xin Lin − *State Key Laboratory of Marine Environmental Science, College of Ocean and Earth Sciences, Xiamen University, Xiamen 361102, P.R. China; Advanced Institute for Marine Studies, Fujian Ocean Innovation Center, Xiamen 361102, P.R. China;* orcid.org/0000-0001-8323-5056; Email: xinlinulm@xmu.edu.cn

Authors

Canru Li − *State Key Laboratory of Marine Environmental Science, College of Ocean and Earth Sciences, Xiamen University, Xiamen 361102, P.R. China*

David A. Hutchins − *Marine and Environmental Biology, University of Southern California, Los Angeles, California 90089, United States*

Haodong Luo − *State Key Laboratory of Marine Environmental Science, College of Ocean and Earth Sciences, Xiamen University, Xiamen 361102, P.R. China*

Ningxin Yan − *State Key Laboratory of Marine Environmental Science, College of Ocean and Earth Sciences, Xiamen University, Xiamen 361102, P.R. China*

Yan Li − *State Key Laboratory of Marine Environmental Science, College of Ocean and Earth Sciences, Xiamen University, Xiamen 361102, P.R. China*

Yuan Jiang − *College of Materials, Higher Educational Key Laboratory for Biomedical Engineering of Fujian Province, Fujian Key Laboratory of Advanced Materials, Xiamen University, Xiamen 361005, P.R. China;* orcid.org/0000-0002-1669-8023

Zhimian Cao − *State Key Laboratory of Marine Environmental Science, College of Ocean and Earth Sciences, Xiamen University, Xiamen 361102, P.R. China*

Minhan Dai − *State Key Laboratory of Marine Environmental Science, College of Ocean and Earth Sciences, Xiamen University, Xiamen 361102, P.R. China;* orcid.org/0000-0003-0550-0701

Complete contact information is available at: https://pubs.acs.org/10.1021/acs.est.6c02131

Author Contributions

X.L., Y.J., and M.D. contributed to the conception of the study; C.L., H.L., and N.Y. performed the experiments; X.L. drafted the manuscript; and D.A.H., Y.L., and Z.C. revised the manuscript. X.L. and C.L. contributed equally.

Notes

No human participants, vertebrate animals, or regulated invertebrates were involved in this study. The research was conducted using laboratory-cultured microalgae and mineral samples; therefore, institutional ethical approval was not required.

The authors declare no competing financial interest.

■ ACKNOWLEDGMENTS

This work was supported by the National Key Research and Development Program of China (NKPs, grant ID: 2025YFF0517300), the National Natural Science Foundation of China (42576144), and the U.S. Sea Grant funding to DAH.

■ REFERENCES

(1) Oschlies, A.; Bach, L. T.; Rickaby, R. E. M.; Satterfield, T.; Webb, R.; Gattuso, J.-P. Climate Targets, Carbon Dioxide Removal, and the Potential Role of Ocean Alkalinity Enhancement. *State Planet* **2023**, *2*, 1−9.

(2) Geerts, L. J. J.; Hylén, A.; Meysman, F. J. R. Review and Syntheses: Ocean Alkalinity Enhancement and Carbon Dioxide Removal Through Marine Enhanced Rock Weathering Using Olivine. *Biogeosciences* **2025**, *22* (2), 355−384.

(3) Behrenfeld, M. J. Climate-Mediated Dance of the Plankton. *Nat. Clim. Change* **2014**, *4* (10), 880−887.

(4) Sheward, R. M. Cycling Carbon with Coccolithophores. *Nat. Geosci.* **2022**, *15* (10), 758−759.
(5) Tréguer, P.; Bowler, C.; Moriceau, B.; Dutkiewicz, S.; Gehlen, M.; Aumont, O.; Bittner, L.; Dugdale, R.; Finkel, Z.; Iudicone, D.; Jahn, O.; Guidi, L.; Lasbleiz, M.; Leblanc, K.; Levy, M.; Pondaven, P. Influence of Diatom Diversity on the Ocean Biological Carbon Pump. *Nat. Geosci.* **2018**, *11* (1), 27−37.
(6) Bach, L. T.; Gill, S. J.; Rickaby, R. E. M.; Gore, S.; Renforth, P. CO_2 Removal with Enhanced Weathering and Ocean Alkalinity Enhancement: Potential Risks and Co-benefits for Marine Pelagic Ecosystems. *Front. Clim.* **2019**, *1*, 7.
(7) Li, C.; Liu, X.; Li, Y.; Jiang, Y.; Guo, X.; Hutchins, D. A.; Ma, J.; Lin, X.; Dai, M. The Interactions between Olivine Dissolution and Phytoplankton in Seawater: Potential Implications for Ocean Alkalinization. *Sci. Total Environ.* **2024**, *912*, No. 168571.
(8) Zhang, E.; Li, Y.; Wang, Y.; Liu, D.; Cong, Y.; Liu, J.; Tang, K.; Jiao, N.; Zheng, Q. Synergistic CO_2 Removal via Enhanced Olivine Weathering and Diatom Growth in the Ocean. *Ocean-Land-Atmos. Res.* **2024**, *3*, No. 0047.
(9) Hutchins, D. A.; Fu, F.-X.; Yang, S.-C.; John, S. G.; Romaniello, S. J.; Andrews, M. G.; Walworth, N. G. Responses of Globally Important Phytoplankton Species to Olivine Dissolution Products and Implications for Carbon Dioxide Removal via Ocean Alkalinity Enhancement. *Biogeosciences* **2023**, *20* (22), 4669−4682.
(10) Gately, J. A.; Kim, S. M.; Jin, B.; Brzezinski, M. A.; Iglesias-Rodriguez, M. D. Coccolithophores and Diatoms Resilient to Ocean Alkalinity Enhancement: A Glimpse of Hope? *Sci. Adv.* **2023**, *9* (24), No. eadg6066.
(11) Bach, L. T.; Boxhammer, T.; Larsen, A.; Hildebrandt, N.; Schulz, K. G.; Riebesell, U. Influence of Plankton Community Structure on the Sinking Velocity of Marine Aggregates. *Global Biogeochem. Cycles* **2016**, *30* (8), 1145−1165.
(12) Bressac, M.; Laurenceau-Cornec, E. C.; Kennedy, F.; Santoro, A. E.; Paul, N. L.; Briggs, N.; Carvalho, F.; Boyd, P. W. Decoding Drivers of Carbon Flux Attenuation in the Oceanic Biological Pump. *Nature* **2024**, *633*, 587−593.
(13) Falkowski, P. The Power of Phytoplankton. *Nature* **2012**, *483*, S17−S20.
(14) Basu, S.; Mackey, K. R. M. Phytoplankton as Key Mediators of the Biological Carbon Pump: Their Responses to a Changing Climate. *Sustainability* **2018**, *10* (3), 869.
(15) Miklasz, K. A.; Denny, M. W. Diatom Sinking Speeds: Improved Predictions and Insight from a Modified Stokes' Law. *Limnol. Oceanogr.* **2010**, *55* (6), 2513−2525.
(16) Durkin, C. A.; Van Mooy, B. A. S.; Dyhrman, S. T.; Buesseler, K. O. Sinking Phytoplankton Associated with Carbon Flux in the Atlantic Ocean. *Limnol. Oceanogr.* **2016**, *61* (4), 1172−1187.
(17) Engel, A.; Szlosek, J.; Abramson, L.; Liu, Z.; Lee, C. Investigating the Effect of Ballasting by $CaCO_3$ in Emiliania huxleyi: I. Formation, Settling Velocities and Physical Properties of Aggregates. *Deep Sea Res. Part II* **2009**, *56* (18), 1396−1407.
(18) Babakhani, P.; Phenrat, T.; Baalousha, M.; Soratana, K.; Peacock, C. L.; Twining, B. S.; Hochella, M. F., Jr. Potential Use of Engineered Nanoparticles in Ocean Fertilization for Large-Scale Atmospheric Carbon Dioxide Removal. *Nat. Nanotechnol.* **2022**, *17* (12), 1342−1351.
(19) Zhang, D.; Wang, Y.; Cai, J.; Pan, J.; Jiang, X.; Jiang, Y. Bio-Manufacturing Technology Based on Diatom Micro- and Nanostructure. *Chin. Sci. Bull.* **2012**, *57* (30), 3836−3849.
(20) Le Moigne, F. A. C.; Pabortsava, K.; Marcinko, C. L. J.; Martin, P.; Sanders, R. J. Where Is Mineral Ballast Important for Surface Export of Particulate Organic Carbon in the Ocean? *Geophys. Res. Lett.* **2014**, *41* (23), 8460−8468.
(21) Falkowski, P.; Scholes, R. J.; Boyle, E.; Canadell, J.; Canfield, D.; Elser, J.; Gruber, N.; Hibbard, K.; Högberg, P.; Linder, S.; Mackenzie, F. T.; Moore, B., III; Pedersen, T.; Rosenthal, Y.; Seitzinger, S.; Smetacek, V.; Steffen, W. The Global Carbon Cycle: A Test of Our Knowledge of Earth as a System. *Science* **2000**, *290* (5490), 291−296.
(22) Zeebe, R. E.; Wolf-Gladrow, D. *CO2 in Seawater: Equilibrium, Kinetics, Isotopes*; Elsevier Oceanography Series, 2001.
(23) Jin, X.; Liu, C. Estimating Coccolithophore PIC:POC Based on Coccosphere and Coccolith Geometry. *J. Geophys. Res. Biogeosci.* **2023**, *128* (4), No. e2022JG007355.
(24) Griffioen, J. Enhanced Weathering of Olivine in Seawater: The Efficiency as Revealed by Thermodynamic Scenario analysis. *Sci. Total Environ.* **2017**, *575*, 536−544.
(25) Frada, M. J.; Bidle, K. D.; Probert, I.; de Vargas, C. In Situ Survey of Life Cycle Phases of the Coccolithophore *Emiliania huxleyi* (Haptophyta). *Environ. Microbiol.* **2012**, *14* (6), 1558−1569.
(26) Müller, M. N.; Trull, T. W.; Hallegraeff, G. M. Differing Responses of Three Southern Ocean Emiliania huxleyi Ecotypes to Changing Seawater Carbonate Chemistry. *Mar. Ecol.: Prog. Ser.* **2015**, *531*, 81−90.
(27) Paasche, E. A Review of the Coccolithophorid Emiliania huxleyi (Prymnesiophyceae), with Particular Reference to Growth, Coccolith Formation, and Calcification-Photosynthesis Interactions. *Phycologia* **2001**, *40* (6), 503−529.
(28) Ritchie, R. J. Consistent Sets of Spectrophotometric Chlorophyll Equations for Acetone, Methanol and Ethanol Solvents. *Photosynth. Res.* **2006**, *89* (1), 27−41.
(29) Bienfang, P. K. SETCOL — A Technologically Simple and Reliable Method for Measuring Phytoplankton Sinking Rates. *Can. J. Fish. Aquat. Sci.* **1981**, *38* (10), 1289−1294.
(30) Jiang, X.; Li, H.; Tong, S.; Gao, K. Nitrogen Limitation Enhanced Calcification and Sinking Rate in the Coccolithophorid *Gephyrocapsa oceanica* Along with its growth being reduced. *Front. Mar. Sci.* **2022**, *9*, No. 834358.
(31) Feng, Y.; Chai, F.; Wells, M. L.; Liao, Y.; Li, P.; Cai, T.; Zhao, T.; Fu, F.; Hutchins, D. A. The Combined Effects of Increased pCO_2 and Warming on a Coastal Phytoplankton Assemblage: From Species Composition to Sinking Rate. *Front. Mar. Sci.* **2021**, *8*, No. 622319.
(32) Petrovich, R. Kinetics of Dissolution of Mechanically Comminuted Rock-Forming Oxides and Silicates—II. Deformation and Dissolution of Oxides and Silicates in the Laboratory and at the Earth's Surface. *Geochim. Cosmochim. Acta* **1981**, *45* (10), 1675−1686.
(33) Ruiz-Agudo, E.; Putnis, C. V.; Rodriguez-Navarro, C.; Putnis, A. Mechanism of Leached Layer Formation During Chemical Weathering of Silicate Minerals. *Geology* **2012**, *40* (10), 947−950.
(34) Segev, E.; Wyche, T. P.; Kim, K. H.; Petersen, J.; Ellebrandt, C.; Vlamakis, H.; Barteneva, N.; Paulson, J. N.; Chai, L.; Clardy, J.; Kolter, R. Dynamic Metabolic Exchange Governs a Marine Algal-Bacterial Interaction. *eLife* **2016**, *5*, No. e17473.
(35) Berry, L.; Taylor, A. R.; Lucken, U.; Ryan, K. P.; Brownlee, C. Calcification and Inorganic Carbon Acquisition in Coccolithophores. *Funct. Plant Biol.* **2002**, *29* (3), 289−299.
(36) Monteiro, F. M.; Bach, L. T.; Brownlee, C.; Bown, P.; Rickaby, R. E. M.; Poulton, A. J.; Tyrrell, T.; Beaufort, L.; Dutkiewicz, S.; Gibbs, S.; Gutowska, M. A.; Lee, R.; Riebesell, U.; Young, J.; Ridgwell, A. Why Marine Phytoplankton. *Calcify. Sci. Adv.* **2016**, *2* (7), No. e1501822.
(37) Ye, J.; Wang, Y.; Li, Q.; Hussain, S.; Chen, S.; Zhou, X.; Hou, S.; Feng, Y. Phagocytosis in Marine Coccolithophore Gephyrocapsa huxleyi: Comparison between Calcified and Non-Calcified Strains. *Biology* **2024**, *13* (5), 310.
(38) Grubb, A. R.; Johns, C. T.; Hayden, M. G.; Subhas, A. V.; Thamatrakoln, K.; Bidle, K. D. Calcification Increases Carbon Supply, Photosynthesis, and Growth in a Globally Distributed Coccolithophore. *Limnol. Oceanogr.* **2024**, *69* (9), 2152−2166.
(39) Sommer, U.; Charalampous, E.; Genitsaris, S.; Moustaka-Gouni, M. Benefits, Costs and Taxonomic Distribution of Marine Phytoplankton Body Size. *J. Plankton Res.* **2016**, *39* (3), 494−508.
(40) Walsby, A. E.; Xypolyta, A. The Form Resistance of Chitan Fibres Attached to the Cells of *Thalassiosira fluviatilis* Hustedt. *Br. Phycol. J.* **1977**, *12* (3), 215−223.
(41) Thamatrakoln, K.; Hildebrand, M. Silicon Uptake in Diatoms Revisited: A Model for Saturable and Nonsaturable Uptake Kinetics

https://doi.org/10.1021/acs.est.6c02131
Environ. Sci. Technol. XXXX, XXX, XXX−XXX

and the Role of Silicon Transporters. *Plant Physiol.* **2008**, *146* (3), 1397−1407.
(42) Brownlee, C.; Taylor, A. Calcification in Coccolithophores: A Cellular Perspective. In *Coccolithophores*; Springer, 2004; pp 31−49.
(43) Ratcliffe, S.; Meyer, E. M.; Walker, C. E.; Knight, M.; McNair, H. M.; Matson, P. G.; Iglesias-Rodriguez, D.; Brzezinski, M.; Langer, G.; Sadekov, A.; Greaves, M.; Brownlee, C.; Curnow, P.; Taylor, A. R.; Wheeler, G. L. Characterization of the Molecular Mechanisms of Silicon Uptake in Coccolithophores. *Environ. Microbiol.* **2022**, *24* (1), 315−330.
(44) Lee, R. B. Y.; Mavridou, D. A. I.; Papadakos, G.; McClelland, H. L. O.; Rickaby, R. E. M. The Uronic Acid Content of Coccolith-Associated Polysaccharides Provides Insight into Coccolithogenesis and Past Climate. *Nat. Commun.* **2016**, *7*, 13144.
(45) Liu, Y.; Cao, X.; Yu, Z.; Song, X.; Qiu, L. Flocculation of Harmful Algal Cells Using Modified Clay: Effects of the Properties of the Clay Suspension. *J. Appl. Phycol.* **2016**, *28* (3), 1623−1633.
(46) Akagi, T. *Biological Weathering and the Environment of the Earth*; Springer Nature, 2024.
(47) Turner, J. T. Zooplankton Fecal Pellets, Marine Snow and Sinking Phytoplankton Blooms. *Aquat. Microb. Ecol.* **2002**, *27* (1), 57−102.
(48) Henson, S.; Le Moigne, F.; Giering, S. Drivers of Carbon Export Efficiency in the Global Ocean. *Global Biogeochem. Cycles* **2019**, *33* (7), 891−903.
(49) Klaas, C.; Archer, D. E. Association of Sinking Organic Matter with Various Types of Mineral Ballast in the Deep Sea: Implications for the Rain Ratio. *Global Biogeochem. Cycles* **2002**, *16* (4), 1063.
(50) Iversen, M. H.; Ploug, H. Ballast Minerals and the Sinking Carbon Flux in the Ocean: Carbon-Specific Respiration Rates and Sinking Velocity of Marine Snow Aggregates. *Biogeosciences* **2010**, *7* (9), 2613−2624.
(51) Cahoon, L. B.; Nearhoof, J. E.; Tilton, C. L. Sediment Grain Size Effect on Benthic Microalgal Biomass in Shallow Aquatic Ecosystems. *Estuaries* **1999**, *22* (3), 735−741.
(52) Blair, N. E.; Rude, P. D.; Aller, R. C. Remineralization Rates, Recycling, and Storage of Carbon in Amazon Shelf Sediments. *Cont. Shelf Res.* **1996**, *16* (6), 753−786.
(53) Graves, C. A.; et al. Sedimentary Carbon on the Continental Shelf: Emerging Capabilities and Research Priorities for Blue Carbon. *Front. Mar. Sci.* **2022**, *9*, No. 926215.
(54) Smith, S. V.; Gattuso, J.-P. Balancing the Oceanic Calcium Carbonate Cycle: Consequences of Variable Water Column. *Aquat. Geochem.* **2011**, *17* (4), 327−337.
(55) Frankignoulle, M.; Canon, C.; Gattuso, J.-P. Marine Calcification as a Source of Carbon Dioxide: Positive Feedback of Increasing Atmospheric CO_2. *Limnol. Oceanogr.* **1994**, *39* (2), 458−462.
(56) Köhler, P.; Abrams, J. F.; Völker, C.; Hauck, J.; Wolf-Gladrow, D. A. Geoengineering Impact of Open Ocean Dissolution of Olivine on Atmospheric CO2, Surface Ocean pH and Marine Biology. *Environ. Res. Lett.* **2013**, *8* (1), No. 014009.
(57) Gattuso, J.-P.; Magnan, A.; Billé, R.; Cheung, W. W. L.; Howes, E. L.; Joos, F.; Allemand, D.; Bopp, L.; Cooley, S. R.; Eakin, C. M.; Hoegh-Guldberg, O.; Kelly, R. P.; Pörtner, H.-O.; Rogers, A. D.; Baxter, J. M.; Laffoley, D.; Osborn, D.; Rankovic, A.; Rochette, J.; Sumaila, U. R.; Treyer, S.; Turley, C. Contrasting Futures for Ocean and Society from Different Anthropogenic CO2 Emissions Scenarios. *Science* **2015**, *349* (6243), No. aac4722.

https://doi.org/10.1021/acs.est.6c02131
Environ. Sci. Technol. XXXX, XXX, XXX−XXX